



# Static response of functionally graded multilayered one-dimensional hexagonal piezoelectric quasicrystal plates using the state vector approach<sup>\*</sup>

Yun-zhi HUANG<sup>1</sup>, Yang LI<sup>2,3</sup>, Lian-zhi YANG<sup>4</sup>, Yang GAO<sup>†‡1</sup>

<sup>1</sup>College of Science, China Agricultural University, Beijing 100083, China

<sup>2</sup>College of Engineering, China Agricultural University, Beijing 100083, China

<sup>3</sup>Department of Mechanical and Power Engineering, Yingkou Institute of Technology, Yingkou 115014, China

<sup>4</sup>School of Civil and Resource Engineering, University of Science and Technology Beijing, Beijing 100083, China

<sup>†</sup>E-mail: gaoyangg@gmail.com

Received Aug. 14, 2018; Revision accepted Nov. 16, 2018; Crosschecked Dec. 26, 2018

**Abstract:** The effect of the non-homogeneity of material properties has been considered the important variation mechanism in the static responses of quasicrystal structures, but the existing theoretical model for it is unable to simulate the material change format beyond the exponential function. In this paper, we create a new model of functionally graded multilayered 1D piezoelectric quasicrystal plates using the state vector approach, in which varying functionally graded electro-elastic properties can be extended from exponential to linear and higher order in the thickness direction. Based on the state equations, an analytical solution for a single plate has been derived, and the result for the corresponding multilayered case is obtained utilizing the propagator matrix method. The present study shows, in particular, that coefficient orders of two varying functions (the power function and the exponential function) of the material gradient provide the ability to tailor the mechanical behaviors in the system's phonon, phason, and electric fields. Moreover, the insensitive points of phonon stress and electric potential under functionally graded effects in the quasicrystal layer are observed. In addition, the influences of stacking sequences and discontinuity of horizontal stress are explored in the simulation by the new model. The results are very useful for the design and understanding of the characterization of functionally graded piezoelectric quasicrystal materials in their applications to multilayered systems.

**Key words:** State vector approach; Functionally graded quasicrystals; Piezoelectric; Plates  
<https://doi.org/10.1631/jzus.A1800472>

**CLC number:** TH113


## 1 Introduction

Quasicrystals (QCs) form an uncommon class of complex metallic alloys with quasiperiodic structures that result from quasiperiodic translational symmetry. Since QCs were first described by Shechtman et al.

(1984), their unique structural characteristics have been the subject of much research. Several desirable properties of QCs have been investigated both experimentally and theoretically, such as high hardness, excellent corrosion and oxidation resistance, low surface energy accompanied by low friction coefficients, high wear resistance, and low electrical and thermal conductivity (Ding et al., 1993; Dubois, 2005; Wang et al., 2005; Gao and Zhao, 2009; Li and Liu, 2012; Li et al., 2013; Yaslan, 2013; Yang et al., 2015; Zhao et al., 2017, 2018). Based on these strengths, QCs have found many applications in the aerospace, solar power, and nuclear fuel industries

<sup>‡</sup> Corresponding author

<sup>\*</sup> Project supported by the National Natural Science Foundation of China (Nos. 11472299 and 51704015) and the China Agricultural University Education Foundation (No. 1101-240001)

 ORCID: Yang GAO, <https://orcid.org/0000-0003-1728-6992>

© Zhejiang University and Springer-Verlag GmbH Germany, part of Springer Nature 2019

(Fan, 2010). Further interest in QCs has been spurred by the analysis of piezoelectric coupling effects within these structures. QCs with piezoelectric effects can realize better performance and higher efficiency when used in smart composite structures and system designs. Due to this significant property of QCs, much research has also been focused on piezoelectric QCs (PQCs) (Fujiwara et al., 1994; Altay and Dökmeci, 2012; Li et al., 2014). Many signal processors under development, such as attenuators, transducers, sensors, and coatings, exploit the potential-coupling effects of piezoelectricity in QCs (Hu et al., 1997; Louzguine-Luzgin and Inoue, 2008; Xu et al., 2017; Sun et al., 2018; Zhou and Li, 2018). Thereafter, increasing attention has been devoted to studying the variation of material properties in PQC.

Stress concentration may be induced by differences in the material properties within multilayered structures (Timoshenko and Goodier, 1970). To overcome this defect and meet design requirements for layered structures, mechanical engineers have developed nonhomogeneous composite materials, also known as functionally graded (FG) materials (Suresh and Mortensen, 1998). In recent years, FG plates and FG multilayered plates have received a great deal of attention. Pan and Han (2005) presented the exact solution for a mathematical model of a FG multilayered magneto-electro-elastic plate using the pseudo-Stroh formalism. The pure bending problem of simply supported transversely isotropic circular plates with elastic compliance coefficients in the FG function was analyzed by Li et al. (2006). Based on 3D thermo-elasticity, Ying et al. (2009) studied the thermal-mechanical response of FG thick plates with one pair of opposite edges simply supported. Yang et al. (2012) analyzed a 3D elastic model of a FG plate with materials showing transverse isotropy subjected to transverse biharmonic loadings. Guo et al. (2016) studied the size-dependent behavior of a FG composite plate based on the modified coupled-stress theory. Mikaeli and Behjat (2016) analyzed the static behavior of thick FG piezoelectric plates using the element-free Galerkin method. Most recently, FG solid circular/annular plates integrated with piezoelectric layers under thermo-electro-mechanical load were studied using the differential quadrature method (Alibeigloo, 2018).

Chan et al. (2002) produced a graded nickel-QC composite by electro-deposition, and the pseudo-Stroh formalism was used to investigate FG QCs with material properties following an exponential distribution (Li et al., 2017). However, FG QCs with gradient parameters that follow a positive symmetrical transverse change have rarely been studied, and very few papers have focused on the static analysis of FG QCs with power function changes of the FG modulus. The objective of this paper is to obtain an exact solution for FG QCs whose material constants vary linearly or by higher-order trends. This exact solution is developed using the state vector approach, which is an effective method for investigating composite structures (Wang et al., 2003).

This paper presents an exact solution for a symmetrical FG multilayered 1D hexagonal PQC plate using the state vector approach. The boundary value problem for this system is converted into an equivalent initial value problem in terms of the mixed formulations. After the propagator matrix and response of the bottom surface are obtained, the exact solution for the corresponding multilayered case is derived. Numerical examples are presented to illustrate the electric-elastic responses of the FG multilayered plates with different stacking sequences subjected to force, displacement, and electric displacement load on their top surface.

## 2 Fundamental equations

Based on the linear elastic theory of 1D PQC (Altay and Dökmeci, 2012), the relationships among strains and displacements, electric field, and its potential are governed by

$$\varepsilon_{ij} = 0.5(u_{i,j} + u_{j,i}), \quad w_{3j} = w_{3,j}, \quad E_j = -\phi_{,j}, \quad (1)$$

where the compact repeated summation conventions are indicated by  $i, j=1, 2, 3$ , and a subscript comma represents partial differentiation with respect to the axis.  $u_i$  and  $w_3$  represent phonon and phason displacement components, respectively,  $\varepsilon_{ij}$  and  $w_{3j}$  denote strains in the phonon and phason fields, respectively, and  $E_j$  and  $\phi$  are the electric field intensity and electric potential, respectively.

Without any body forces and electric charge

densities, the static equilibrium equations can be expressed as

$$\sigma_{ij,j} = 0, H_{3j,j} = 0, D_{j,j} = 0, \quad (2)$$

where phonon stresses, phason stresses, and electric displacements are denoted by  $\sigma_{ij}$ ,  $H_{3j}$ , and  $D_j$ , respectively.

Referred to a coordinate system  $(x_1, x_2, x_3)$ , the atomic arrangement of 1D hexagonal QCs is periodic in the  $x_1$ - $x_2$  plane and quasi-periodic along the  $x_3$  axis. The coupled constitutive equations with vertically polarized piezoelectric effect (Li et al., 2014) take the following forms:

$$(3) \quad \begin{cases} \sigma_{11} = C_{11}\varepsilon_{11} + C_{12}\varepsilon_{22} + C_{13}\varepsilon_{33} + R_1w_{33} - e_{31}E_3, \\ \sigma_{22} = C_{12}\varepsilon_{11} + C_{11}\varepsilon_{22} + C_{13}\varepsilon_{33} + R_1w_{33} - e_{31}E_3, \\ \sigma_{33} = C_{13}\varepsilon_{11} + C_{13}\varepsilon_{22} + C_{33}\varepsilon_{33} + R_2w_{33} - e_{33}E_3, \\ \sigma_{23} = \sigma_{32} = 2C_{44}\varepsilon_{23} + R_3w_{32} - e_{15}E_2, \\ \sigma_{31} = \sigma_{13} = 2C_{44}\varepsilon_{13} + R_3w_{31} - e_{15}E_1, \\ \sigma_{12} = \sigma_{21} = 2C_{66}\varepsilon_{12}, \\ H_{31} = 2R_3\varepsilon_{13} + K_2w_{31} - d_{15}E_1, \\ H_{32} = 2R_3\varepsilon_{23} + K_2w_{32} - d_{15}E_2, \\ H_{33} = 2R_3\varepsilon_{12} + R_2\varepsilon_{33} + K_1w_{33} - d_{33}E_3, \\ D_1 = 2e_{15}\varepsilon_{13} + d_{15}w_{31} + \lambda_{11}E_1, \\ D_2 = 2e_{15}\varepsilon_{23} + d_{15}w_{32} + \lambda_{11}E_2, \\ D_3 = e_{31}(\varepsilon_{11} + \varepsilon_{22}) + e_{33}\varepsilon_{33} + d_{33}w_{33} + \lambda_{33}E_3. \end{cases}$$

The constants involved in Eq. (3) are the phonon elastic moduli  $C_{ij}$  with  $C_{66}=(C_{11}-C_{22})/2$ , the phason elastic moduli  $K_1$  and  $K_2$ , the phonon-phason coupling elastic moduli  $R_1$ ,  $R_2$ , and  $R_3$ , the dielectric moduli  $\lambda_{11}$  and  $\lambda_{33}$ , the phonon piezoelectric moduli  $e_{15}$ ,  $e_{31}$ , and  $e_{33}$ , and the phason field piezoelectric moduli  $d_{15}$  and  $d_{33}$ . It is noted that various uncoupled cases can be removed from Eq. (3) by setting the appropriate coefficients to be zero. For instance, the constitutive equations of the crystal are obtained by letting terms  $R_1$ ,  $R_2$ , and  $R_3$  vanish.

### 3 Problem description and state vector formulation

A simply supported FG multilayered 1D PQC plate is assumed to be of total thickness  $z=H$  in the

vertical direction and horizontal dimensions  $x \times y = L_x \times L_y$  in the region of the plane as depicted in Fig. 1. The relationship between the local material coordinate system and the global Cartesian coordinate system of the plate is assumed as  $(x_1, x_2, x_3) = (x, y, z)$ . One of the four corners of the bottom surface is used as the origin of the Cartesian coordinate system, and the plate occupies the positive region. The  $j$ th layer is denoted by  $j$  in the layered plate, and its lower and upper surfaces are defined as  $z_{j-1}$  and  $z_j$ , respectively, with thickness  $h_j = z_j - z_{j-1}$ . It is assumed that the displacements and  $z$ -direction tractions are continuous across the layer interface, and the homogeneous material is at rest and unstressed in its original natural reference state.

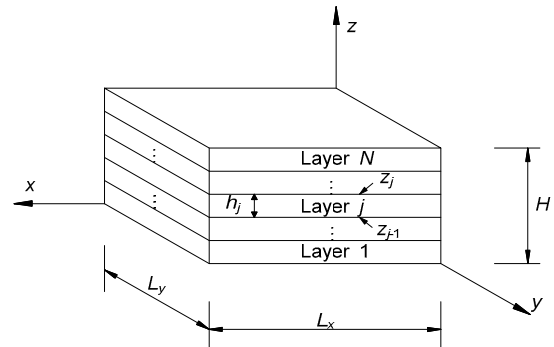


Fig. 1 FG multilayered 1D PQC plate

The basic Eqs. (1)–(3) consisting of 17 unknowns and 17 equations are constructed, where the 17 unknowns are composed of three phonon displacements, one phason displacement, six phonon stresses, three phason stresses, three electric displacements, and one electric potential.

According to the mixed formulation of solid mechanics (Wang et al., 2003), the state vector approach sets out-of-plane unknowns ( $u_x, u_y, u_z, \sigma_{zz}, D_z, H_{zz}, \sigma_{xz}, \sigma_{yz}, \phi$ , and  $w_z$ ) as basic variables, which are defined as primary variables  $\theta_1$ . Furthermore, the in-plane unknowns ( $\sigma_{xx}, \sigma_{yy}, \sigma_{xy}, D_x, D_y, H_{zx}$ , and  $H_{zy}$ ) are incorporated into additional variables, which are called the secondary variables  $\theta_2$ . Then, the state vector equations for 1D PQC can be established by combining the basic unknowns of three governing equations in Eqs. (1)–(3), which are expressed as



### 4 Analytical solutions for FG multilayered 1D PQC plate

The theoretical solutions of multilayered plates under various boundary conditions have been obtained by using the state vector approach (Sheng et al., 2007; Hu and Liu, 2015; Qing et al., 2017). For free/clamped boundary conditions, related components of displacement or stress are assumed as zero at edges. To satisfy these conditions, the boundary functions need to be added to the expressions of unknowns, which are introduced into the state equation as non-homogeneous terms. Therefore, the total state equation is non-homogeneous.

In this section, the state vector equations are used to obtain an analytical solution for simply supported FG multilayered 1D PQC plates. This boundary condition is not only concise in expression, but also avoids non-homogeneous terms in the derivation process compared with other boundary conditions (Levinson and Cooke, 1983). Li et al. (2017) and Sun et al. (2018) presented the simply supported boundary conditions of multilayered QCs plates. Similarly, the simply supported boundary conditions of the developed model can be presented as

$$\begin{cases} x = 0 \text{ and } x = L_x: u_y = u_z = \phi = w_z = \sigma_{xx} = 0; \\ y = 0 \text{ and } y = L_y: u_x = u_z = \phi = w_z = \sigma_{yy} = 0. \end{cases} \quad (11)$$

In the absence of body forces and electric charge density, the state variables for a FG multilayered 1D PQC plate under simply supported lateral boundary conditions are assumed to be

$$\begin{bmatrix} u_x \\ u_y \\ D_z \\ H_{zz} \\ \sigma_{zz} \\ \sigma_{xz} \\ \sigma_{yz} \\ \phi \\ w_z \\ u_z \end{bmatrix} = \sum_{m=1}^{\infty} \sum_{n=1}^{\infty} \begin{bmatrix} \bar{u}_{xmn}(z) \cos(px) \sin(qy) \\ \bar{u}_{ymn}(z) \sin(px) \cos(qy) \\ \bar{D}_{zmn}(z) \sin(px) \sin(qy) \\ \bar{H}_{zzmn}(z) \sin(px) \sin(qy) \\ \bar{\sigma}_{zzmn}(z) \sin(px) \sin(qy) \\ \bar{\sigma}_{xzm}(z) \cos(px) \sin(qy) \\ \bar{\sigma}_{yzm}(z) \sin(px) \cos(qy) \\ \bar{\phi}_{mn}(z) \sin(px) \sin(qy) \\ \bar{w}_{zmn}(z) \sin(px) \sin(qy) \\ \bar{u}_{zmn}(z) \sin(px) \sin(qy) \end{bmatrix}, \quad (12)$$

where  $p=m\pi/L_x$ ,  $q=n\pi/L_y$ , in which  $m$  and  $n$  are the superposition numbers.

Substituting Eq. (12) into Eq. (4), a system of ordinary differential equations is obtained in the following matrix forms:

$$\frac{\partial \bar{\theta}_{1mn}}{\partial z} = \bar{K}_F \bar{\theta}_{1mn}, \quad \bar{\theta}_{2mn} = \bar{L}_F \bar{\theta}_{1mn}, \quad (13)$$

where  $\bar{\theta}_{1mn} = [\bar{u}_{xmn} \quad \bar{u}_{ymn} \quad \bar{D}_{zmn} \quad \bar{H}_{zzmn} \quad \bar{\sigma}_{zzmn} \quad \bar{\sigma}_{xzm} \quad \bar{\sigma}_{yzm} \quad \bar{\phi}_{mn} \quad \bar{w}_{zmn} \quad \bar{u}_{zmn}]^T$ ,  $\bar{\theta}_{2mn} = [\bar{\sigma}_{xxmn} \quad \bar{\sigma}_{yy} \quad \bar{\sigma}_{xymn} \quad \bar{D}_{xmn} \quad \bar{D}_{ymn} \quad \bar{H}_{zxm} \quad \bar{H}_{zym}]^T$ . Then the solution of the  $j$ th layer in Eq. (13) is found to be

$$\begin{aligned} \bar{\theta}_{1mn}(z) &= \exp[\bar{K}_F(z-z_{j-1})] \bar{\theta}_{1mn}(z_{j-1}) \\ &= \mathbf{Q}(z-z_{j-1}) \bar{\theta}_{1mn}(z_{j-1}), \quad z_{j-1} \leq z \leq z_j, \end{aligned} \quad (14)$$

where the exponential matrix  $\exp[\bar{K}_F(z-z_{j-1})]$  is the (10×10) propagator matrix. For each layer of FG multilayered 1D PQC plates, we also use the following equations to determine the other variables:

$$\begin{cases} \bar{\theta}_{1mn}(z_1) = \mathbf{Q}_1(h_1) \bar{\theta}_{1mn}(0), \\ \bar{\theta}_{1mn}(z_2) = \mathbf{Q}_2(h_2) \bar{\theta}_{1mn}(z_1), \\ \vdots \\ \bar{\theta}_{1mn}(z_N) = \mathbf{Q}_N(h_N) \bar{\theta}_{1mn}(z_{N-1}). \end{cases} \quad (15)$$

The continuity conditions at the interface between the  $j$ th and  $(j+1)$ th layers are assumed, and then the computational equation of the physical quantities on the top surface is

$$\bar{\theta}_{1mn}(z_N) = \mathbf{P} \bar{\theta}_{1mn}(0), \quad (16)$$

where

$$\mathbf{P} = \mathbf{Q}_N(h_N) \mathbf{Q}_{N-1}(h_{N-1}) \cdots \mathbf{Q}_2(h_2) \mathbf{Q}_1(h_1). \quad (17)$$

For FG multilayered 1D PQC plates, the primary variables can be divided into a displacement vector and a traction vector. We rewrite Eq. (16) as follows:

$$\begin{bmatrix} \bar{U}_{mn}(z_N) \\ \bar{T}_{mn}(z_N) \end{bmatrix} = \begin{bmatrix} N_{11} & N_{12} \\ N_{21} & N_{22} \end{bmatrix} \begin{bmatrix} \bar{U}_{mn}(0) \\ \bar{T}_{mn}(0) \end{bmatrix}, \quad (18)$$

where  $\bar{U}_{mn} = [\bar{u}_{xmn} \ \bar{u}_{ymn} \ \bar{\phi}_{mn} \ \bar{w}_{zmn} \ \bar{u}_{zmn}]^T$ ,  $\bar{T}_{mn} = [\bar{D}_{zmn} \ \bar{H}_{zzmn} \ \bar{\sigma}_{zzmn} \ \bar{\sigma}_{xzmn} \ \bar{\sigma}_{yzmn}]^T$ .  $N_{kl}$  is a recombined matrix corresponding to  $\bar{U}_{mn}$  and  $\bar{T}_{mn}$ , which are rearranged variables of  $\bar{\theta}_{1mn}$  in Eq. (16).

Three loads ( $\sigma_{zz}$ ,  $D_z$ , and  $u_z$ ) are separately applied on the top surface ( $z=H$ ) of the plate with the bottom surface traction free. We can expand them into an infinite double Fourier series, and then add the responses together by term:

$$\begin{bmatrix} \bar{\sigma}_{zzmn} \\ \bar{D}_{zmn} \\ \bar{u}_{zmn} \end{bmatrix} = \frac{4}{L_x L_y} \int_0^{L_x} \int_0^{L_y} \begin{bmatrix} \sigma_{zz} \\ D_z \\ u_z \end{bmatrix} \sin(px) \sin(qy) dx dy. \quad (19)$$

Solving the above equations, the results of Eq. (18) are

$$\begin{aligned} \bar{U}_{mn}(z_N) &= (N_{12} - N_{11}N_{21}^{-1}N_{22})\bar{T}_{mn}(0) + N_{11}N_{21}^{-1}\bar{T}_{mn}(z_N), \\ \bar{U}_{mn}(0) &= N_{21}^{-1}[\bar{T}_{mn}(z_N) - N_{22}\bar{T}_{mn}(0)]. \end{aligned} \quad (20)$$

By employing Eqs. (15) and (16), the solutions of the generalized displacements and tractions of the interior layer are evaluated, and those of the secondary variables are obtained by Eq. (13).

## 5 Numerical examples

Based on the formulations presented above, the responses of a simply supported FG multilayered 1D PQC plate with embedded and/or surface-banded piezoelectric layers are studied in this section. Both side lengths ( $L_x$ ,  $L_y$ ) of the model are 1 m and the total thickness  $H$  is taken as 0.3 m. The piezoelectric crystal material BaTiO<sub>3</sub> and QCs material Al-Ni-Co are transversely isotropic solids abbreviated as B and A, respectively, and their material constants are shown in Tables 1 and 2 (Fan, 2013; Sladek et al., 2013). Note that the coefficients  $K_1$ ,  $K_2$ ,  $R_1$ ,  $R_2$ , and  $R_3$  in the crystal BaTiO<sub>3</sub> layer are assumed to have very small values (about  $10^{-10}$  of the interrelated values in the Al-Ni-Co layer), which are able to meet the requirements for completeness of the system matrices. The factors influencing the mechanical behaviors are

discussed below. They are the FG coefficient, and the loading and stacking sequences, respectively. The given non-homogeneous formats of the FG coefficients (Chen and Lee, 2003; Li et al., 2017) are considered as follows:

$$F_1(z) = \left( \frac{H-z}{H} \right)^f, \quad F_2(z) = \exp(\eta z), \quad (21)$$

where  $F_1(z)$  simulates power function changes, and exponential change is modeled as  $F_2(z)$ . The non-homogeneity factor or gradient index is indicated by  $f$  and  $\eta$  in Eq. (21), respectively.

**Table 1 Material constants of Al-Ni-Co**

Parameter	Fan (2013)'s value
Phonon elastic ( $\times 10^9$ N/m <sup>2</sup> )	$C_{11}=234.3, C_{12}=57.4, C_{13}=66.6,$ $C_{33}=232.2, C_{44}=70.2, C_{66}=88.5$
Phason elastic ( $\times 10^9$ N/m <sup>2</sup> )	$K_1=122, K_2=24$
Phonon-phason ( $\times 10^9$ N/m <sup>2</sup> )	$R_1=8.85, R_2=8.85, R_3=8.85$
Piezoelectric (C/m <sup>2</sup> )	$e_{15}=-0.138, e_{31}=-0.160, e_{33}=0.347,$ $d_{15}=-0.160, d_{33}=0.350$
Dielectric ( $\times 10^{-12}$ F/m)	$\lambda_{11}=82.6, \lambda_{33}=90.3$

**Table 2 Material constants of BaTiO<sub>3</sub>**

Parameter	Sladek et al. (2013)'s value
Phonon elastic ( $\times 10^9$ N/m <sup>2</sup> )	$C_{11}=166, C_{12}=77, C_{13}=78, C_{33}=162,$ $C_{44}=43, C_{66}=44.5$
Piezoelectric (C/m <sup>2</sup> )	$e_{15}=11.6, e_{31}=-4.4, e_{33}=18.6, d_{15}=0,$ $d_{33}=0$
Dielectric ( $\times 10^{-9}$ F/m)	$\lambda_{11}=11.2, \lambda_{33}=12.6$

Meanwhile, we only investigate two three-layer sandwich plates and two four-layer multilayered plates, whose stacking sequences can be expressed as: (a) A/B/A (QCs-skin-layer); (b) B/A/B (QCs-core-layer); (c) A/B/B/A; (d) B/A/A/B. The thickness of each layer in one kind of structure is equal. The thickness is 0.1 m in the three-layer plates (a) and (b) and 0.075 m in the four-layer plates (c) and (d). The material properties of the middle two layers in (c) are the same in order to compare them with structure (d).

We present the standard of numerical convergence of the results, which are obtained by the  $m$ th and  $n$ th superposition of the Fourier series. If the relative error of the result is less than a certain value

when  $m$  and  $n$  are large enough, the numerical result is convergent (Móricz, 1989). The numerical results indicate that when  $m \geq 11$  and  $n \geq 11$ , the relative error of the result is less than 0.01%. Corresponding charts are omitted for brevity. Thus, the results are shown to converge.

In addition, the research in this section is classified into three types of vertical loading in Eq. (19) applied on the top surface of the plate ( $z=H$ ). These loads are assumed as single sinusoidal loads, such as  $\sigma_{zz} = \bar{\sigma}_{zz} \sin(\pi x / L_x) \sin(\pi y / L_y)$ , so we can obtain static responses by taking the first item of the Fourier series ( $m=n=1$ ). The initial values of loading are

$$\begin{cases} \text{Load I: } \bar{\sigma}_{zz}(H) = 1 \text{ N/m}^2, \\ \text{Load II: } \bar{D}_z(H) = 1 \text{ C/m}^2, \\ \text{Load III: } \bar{u}_z(H) = 1 \times 10^{-3} \text{ m}, \end{cases} \quad (22)$$

where phonon stress, electric displacement, and phonon displacement in the thickness direction are expressed as  $\bar{\sigma}_{zz}$ ,  $\bar{D}_z$ , and  $\bar{u}_z$ , respectively, while all other traction components are set to zero on the top and bottom surfaces, e.g.  $\bar{\sigma}_{xz} = 0$ ,  $\bar{\sigma}_{yz} = 0$ ,  $\bar{H}_{zz} = 0$ , and  $\bar{D}_z = 0$ .

### 5.1 Mechanical load

In this part, two numerical examples of rectangular plates are carried out to verify the accuracy of the proposed method and the numeric solution. Under the top surface Load I, the phonon and phason responses of the plate along the  $z$ -direction are considered by showing the results on the vertical line with fixed horizontal coordinates at  $(x, y) = (0.75L_x, 0.25L_y)$ . Firstly, by neglecting the phason field effect, we obtain the phonon displacements  $u_x$  and  $u_z$  in the single-layer plate with different gradient factors  $\eta$  in  $F_2(z)$ . In the numerical calculation, the dimensions of the plate are  $L_x:L_y:H=3:3:1$ , and the material properties are taken from Guo et al. (2016). The results of the state vector approach have a good accordance with those of Guo et al. (2016) in Fig. 2. In particular, Fig. 2b demonstrates that  $u_z$  decreases with the increasing gradient factor  $\eta$ . Secondly, phonon stress  $\sigma_{zz}$  and phason stress  $H_{zz}$  in the multilayered PQC plates without gradient factor  $\eta$  are obtained by using materials properties and geometry sizes presented by Sun

et al. (2018). Fig. 3 presents the results with those by Sun et al. (2018), which are also consistent with the thickness direction for the A/B/A and B/A/B models. More specially, as shown in Fig. 3a,  $\sigma_{zz}$  at the top and bottom surfaces meets the requirements of the boundary conditions.  $H_{zz}$  is non-zero in the QCs layer, and it becomes exactly zero in the crystal layer in Fig. 3b.

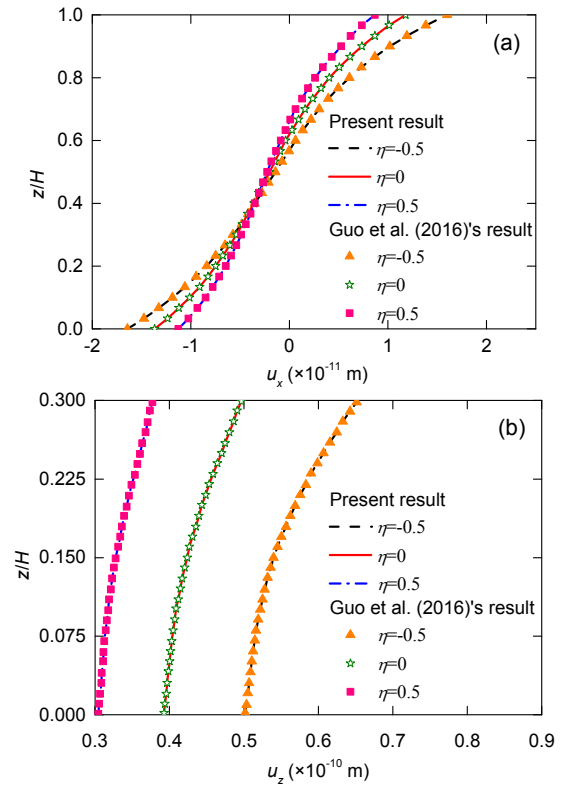


**Fig. 2** Variation of the phonon displacement components in the simple plate under different gradient factors  $\eta$  in  $F_2(z)$

(a)  $u_x$  in single-layer plate; (b)  $u_z$  in single-layer plate

The focus of our analysis is on static behavior in which the variation of QCs material properties is linear and of higher order in  $F_1(z)$ . Similarly, static responses are calculated in the thickness direction, with fixed horizontal coordinates  $(x, y) = (0.75L_x, 0.75L_y)$ . The crystal layers are utilized as sensors whose material properties are homogeneous. The symmetrical variations of the physical quantities along the thickness direction of the layered plates are shown for five values of  $f$  in Figs. 4a and 4b, where  $f=1, 2$  can stimulate the linear and second-order changes of the FG coefficient separately. For  $z$  ranging from 0.225 to 0.3 m in Fig. 4a, for example, the

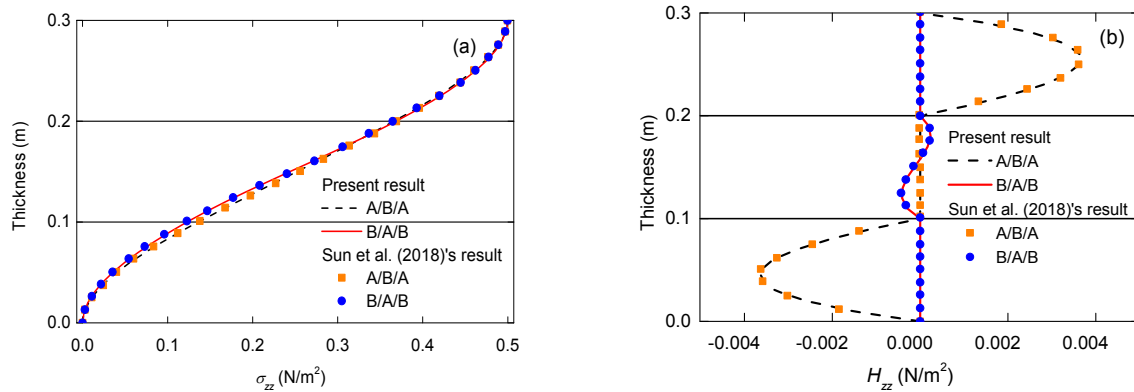


**Fig. 3** Variation of the phonon and phason stress components in the three-layer plate  
 (a)  $\sigma_{zz}$  in A/B/A and B/A/B plates; (b)  $H_{zz}$  in A/B/A and B/A/B plates

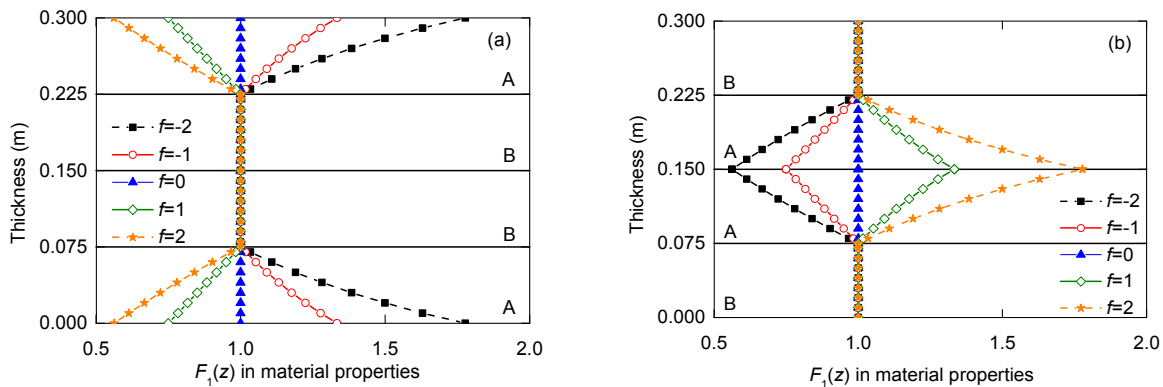


**Fig. 4** Variation of the FG multilayered proportional coefficient for change of gradient factor  $f$  in  $F_1(z)$   
 (a) Proportional factor in A/B/B/A plate; (b) Proportional factor in B/A/A/B plate

coefficient is the non-homogeneous factor:  $F_1(z) = \{[H - (z - 0.225)] / H\}^f$ , and other factors can be calculated in a similar way.

Figs. 5a and 5b show, respectively, the variation of the phonon displacements  $u_z$  along the thickness direction in the A/B/B/A and B/A/A/B plates.  $u_z$  increases with decreasing gradient factor  $f$  in the B/A/A/B plate, while the opposite trend occurs in the A/B/B/A plate. These features illustrate that some relations exist between the gradient factor and the stiffness of the plate. Figs. 5c and 5d give variation of the phonon stress  $\sigma_{zz}$  for both the A/B/B/A and B/A/A/B plates, respectively. The material non-homogeneity only has a small influence on  $\sigma_{zz}$  in the PQC field. For a multilayered plate, Li et al. (2017) also reported that there was almost no difference of  $\sigma_{zz}$  between two stacking schemes.

The variations of phason displacements  $w_z$  and phason stress  $H_{zz}$  in the  $z$ -direction for different structures are plotted in Figs. 6a–6d, respectively. The

magnitudes of phason quantities are very small in the piezoelectric BaTiO<sub>3</sub> layers, owing to the fact that the phason coefficients are almost zero for piezoelectric crystal materials. As for  $w_z$  in Figs. 6a and 6b, its absolute value increases with the gradient factor  $f$  in the QCs layers. It is also interesting to note from Fig. 6d that the phason stresses are positive when  $f < 0$ , while they are negative by setting  $f$  to a positive value in the QCs layer.

Another easily observed example of electric potential  $\phi$  in Fig. 7 (p.142) is that  $\phi$  is insensitive for the FG effect at the middle plane of the plate. Despite the discontinuities of different material properties, that situation is between the upper and lower parts of the same material. It can be defined as the insensitive point of  $\phi$  under the FG effect due to the particular nature of the structure. It is indicated that  $\phi$  is almost constant at that point within the layer where the material properties of QCs may change differently owing to external influences, which can be regarded as a good interface in engineering design.



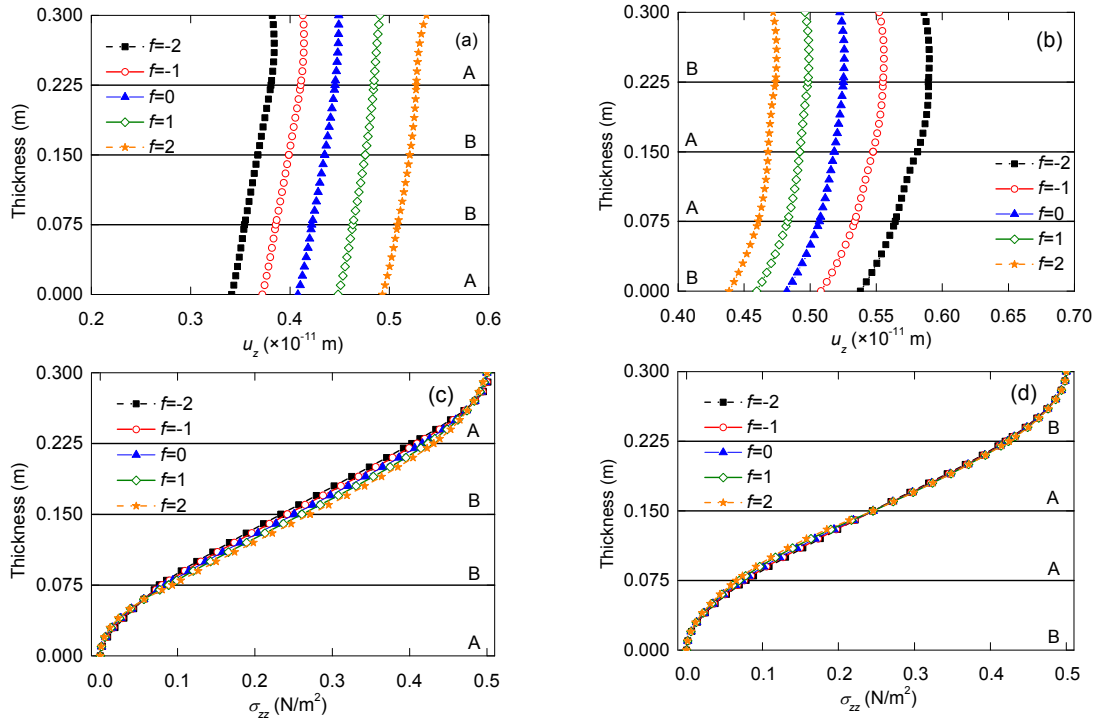


**Fig. 5 Variation of elastic components along thickness direction under Load I**  
 (a)  $u_z$  in A/B/B/A plate; (b)  $u_z$  in B/A/A/B plate; (c)  $\sigma_{zz}$  in A/B/B/A plate; (d)  $\sigma_{zz}$  in B/A/A/B plate

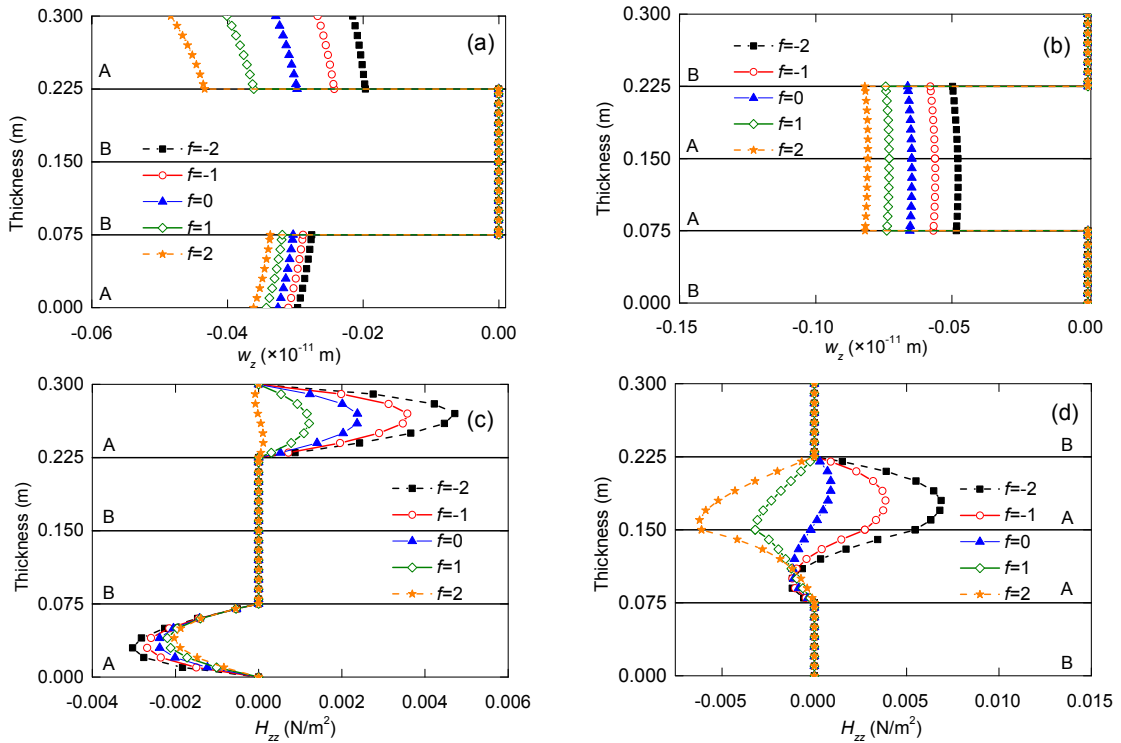


**Fig. 6 Variation of phason components along thickness direction under Load I**  
 (a)  $w_z$  in A/B/B/A plate; (b)  $w_z$  in B/A/A/B plate; (c)  $H_{zz}$  in A/B/B/A plate; (d)  $H_{zz}$  in B/A/A/B plate

### 5.2 Electric load

Under the top surface Load II, the variations of electric displacement  $D_z$  and electric potential  $\phi$  along the thickness direction for a range of values of  $f$  are presented in Figs. 8a and 8b as well as in Figs. 8c and 8d, respectively.  $\phi$  is completely different between the two structures, which in A/B/B/A is roughly two orders larger than in B/A/A/B.  $\phi$  is also not affected much by  $f$  in the BaTiO<sub>3</sub> layer. Moreover, Figs. 8b

and 8c show that  $D_z$  and  $\phi$  are very small from the second to the fourth layers. Because the dielectric constants in the QCs layer are much smaller than those in the BaTiO<sub>3</sub> layers,  $D_z$  and  $\phi$  are close to zero at the bottom of the first layer.

Figs. 9a–9d show, respectively, the variations of phonon displacement  $u_x$  and phonon stress  $\sigma_{xx}$  in the  $z$ -direction for the two multilayered plates. By comparison with the structural parameters of piezoelectric FG materials on in-plane displacement and stress

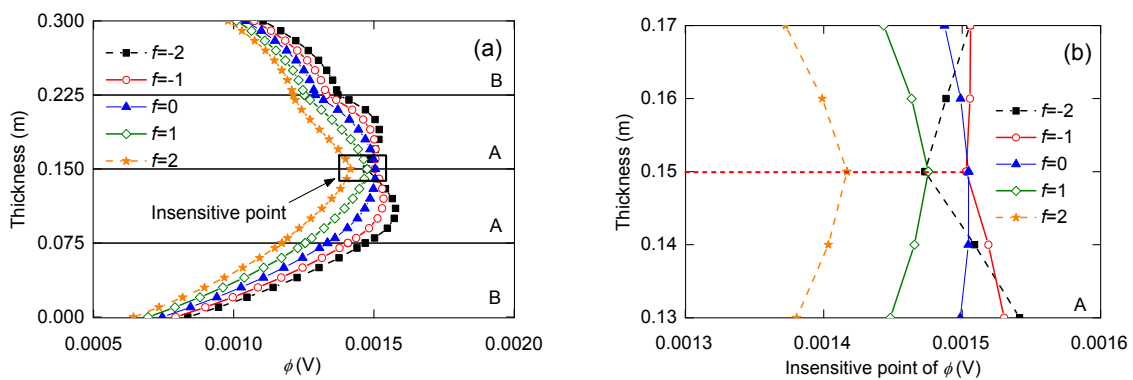


**Fig. 7** Variation of electric potential along thickness direction under Load I  
(a)  $\phi$  in B/A/A/B plate; (b) Insensitive point of  $\phi$  in Fig. 7a

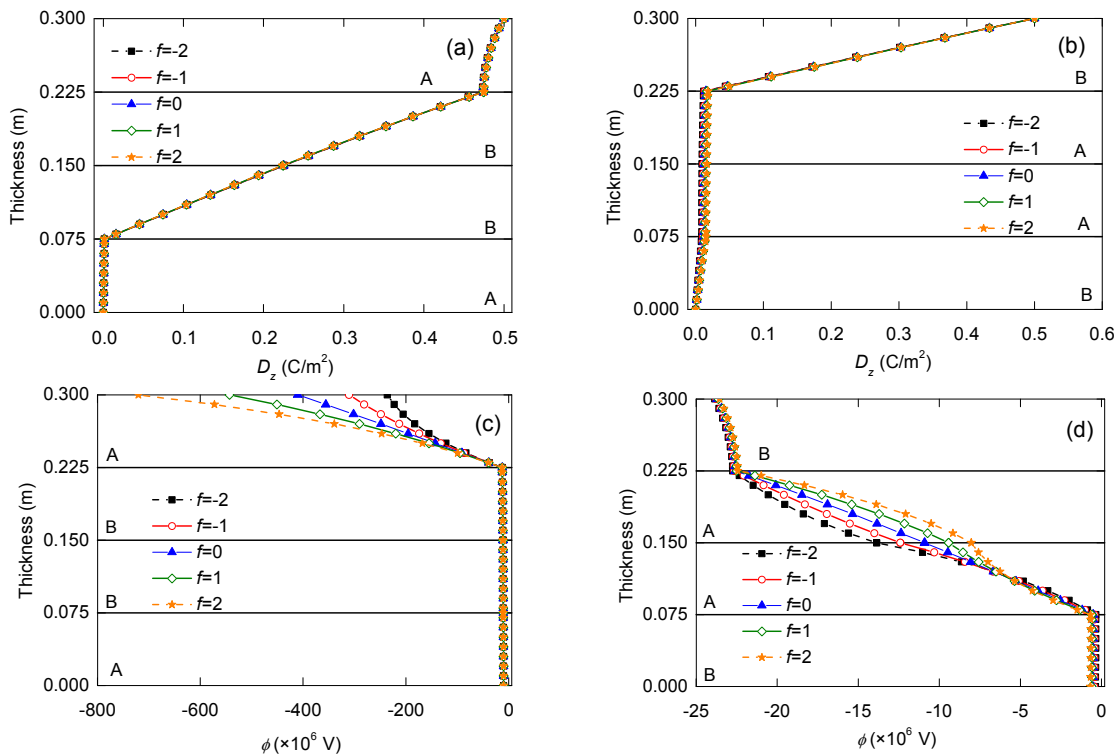


**Fig. 8** Variation of electric components along thickness direction under Load II  
(a)  $D_z$  in A/B/B/A plate; (b)  $D_z$  in B/A/A/B plate; (c)  $\phi$  in A/B/B/A plate; (d)  $\phi$  in B/A/A/B plate

components in the B/A/A/B plate, the larger influence is induced in the A/B/B/A plate. Such a phenomenon is similar to that shown in Figs. 8c and 8d, indicating that  $u_x$ ,  $\sigma_{xx}$ , and  $\phi$  are more sensitive to the stacking sequence. In addition, the in-plane stresses  $\sigma_{xx}$  in Figs. 9c and 9d are discontinuous across the interfaces. While only partial stresses presented in state equations are considered based on classical laminate theory, in fact, the stress state also includes interlayer stresses, which are usually strong between the interfaces. High inter-laminar stress is regarded as one of the specific failure mechanisms of composite materials in engineering applications. Abrupt changes in the

surface of  $z=0.225$  m in Fig. 9c and 9d between two adjacent layers may result in delamination of the ones under vertical loading. In engineering practice, the way to restrain delamination between layers is to enhance the bonding at the interface and increase the number of layers. Also, the insensitive point of  $\sigma_{zz}$  occurs at  $z=0.250$  m in the QCs layer in Fig. 9f, where a stable situation for  $\sigma_{zz}$  can be observed.

### 5.3 Initial displacement

Some physical components are calculated for applying Load III (the initial displacement  $u_z$  on its top surface), which is the same for different gradient

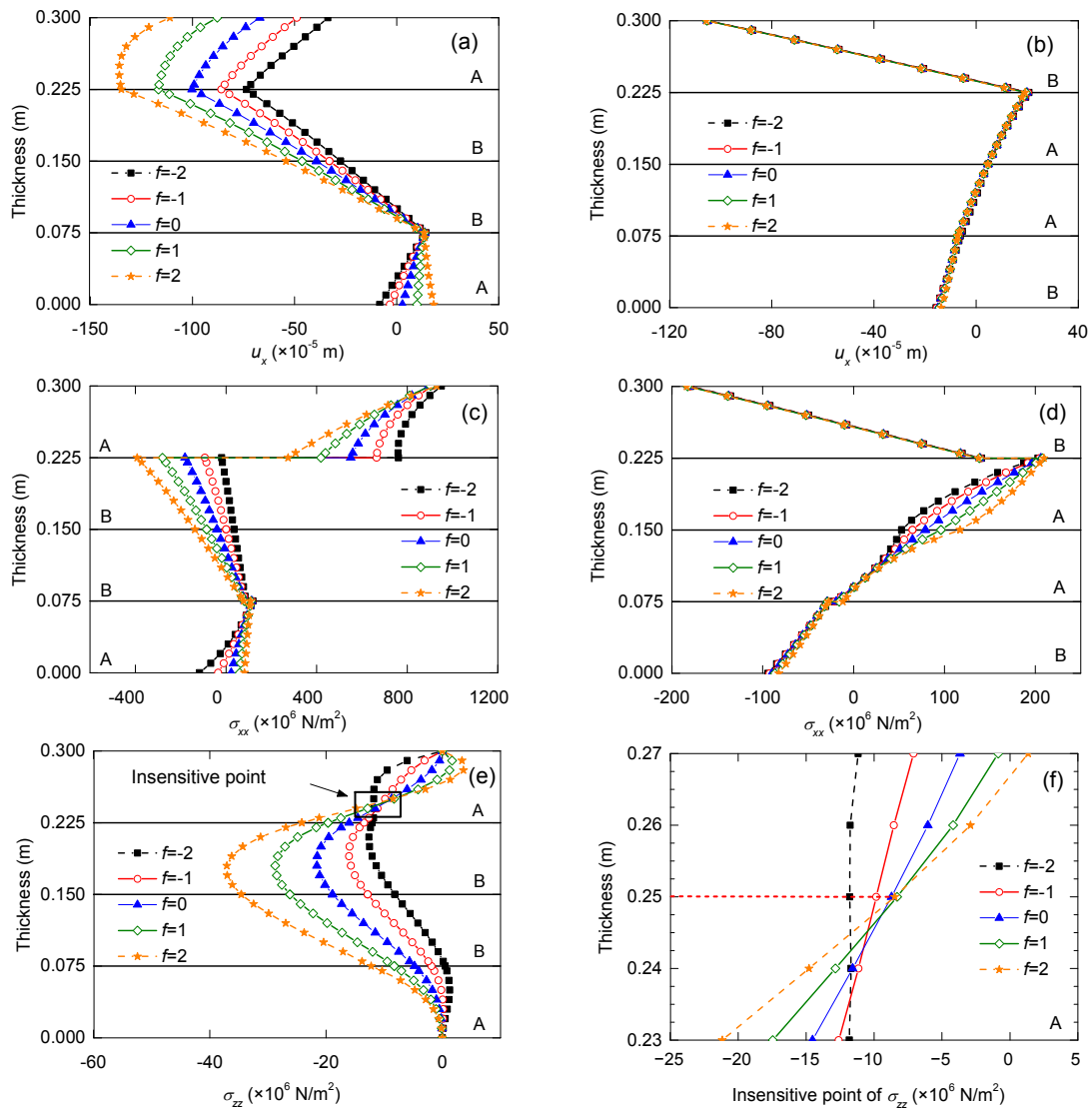


**Fig. 9** Variation of elastic components along thickness direction under Load II

(a)  $u_x (=u_y)$  in A/B/B/A plate; (b)  $u_x (=u_y)$  in B/A/A/B plate; (c)  $\sigma_{xx} (= \sigma_{yy})$  in A/B/B/A plate; (d)  $\sigma_{xx} (= \sigma_{yy})$  in B/A/A/B plate; (e)  $\sigma_{zz}$  in A/B/B/A plate; (f) Insensitive point of  $\sigma_{zz}$  in Fig. 9e

factors. Table 3 compares the maximum values of horizontal physical quantities on the vertical line in the A/B/B/A plate for the variations of gradient factor  $f$  from  $-2$  to  $2$ , separately. As can be seen, a positive effect of the gradient parameter is shown, in which the maximum absolute values of the horizontal physical components decrease with increasing factor  $f$ . The horizontal stress components ( $\sigma_{xx}$ ,  $\sigma_{xy}$ , and  $\sigma_{yz}$ ) change obviously with  $f$ . However, the influence of  $f$  is slight on  $u_x$ . Moreover, Fig. 10a depicts the variations of  $\phi$  under  $u_z$  loading in the B/A/A/B plate. Under the

initial displacement, there is an insensitive point of  $\phi$  in Fig. 10b resembling those in Fig. 7a and Fig. 8d, which indicates that insensitive points of  $\phi$  are predicted in phonon and electric fields.

### 6 Conclusions

In this paper, the static response of a FG multilayered 1D PQC simply-supported plate subjected to mechanical and electrical load and initial displacement on its top surface is studied by the state vector approach. By introducing ten state variables in the phonon, phason, and electric fields, tenth-order state equations are derived. After a general solution is obtained for each layer, the states of the corresponding multilayered structures can be accurately modelled using the propagator matrix method. Analytical solutions gained by the application of the proposed method and results given in the literature are in relatively good agreement with each other.

It is constructive to analyze FG multilayered plate models using the state vector approach, since the approach can be generalized to investigate other materials that are non-homogeneous in the thickness direction. In addition, the FG coefficients in the formulations can be designed in different forms as desired, so that the model can give solutions for the variations of other material properties.

In numerical examples, two multilayered plates made of crystals and QCs are analyzed, with the material properties varying in the thickness direction within the QCs layers. Different FG coefficients lead to various effects in the phonon, phason, and electric fields. With the higher-order coefficients in power function, the feasible ranges of the component values

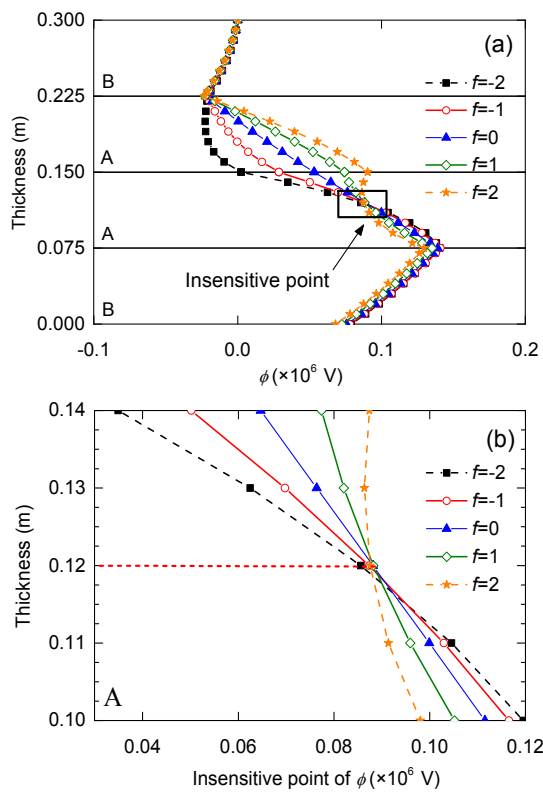


**Fig. 10** Variation of elastic components along thickness direction under Load III (a)  $\phi$  in A/B/B/A plate; (b) Insensitive point of  $\phi$  in Fig. 10a

**Table 3** Maximum absolute values of horizontal physical components along the  $z$  direction for Load III

Gradient factor	$u_x$ ( $\times 10^{-5}$ m)	$\sigma_{xx}$ ( $\times 10^6$ N/m <sup>2</sup> )	$\sigma_{xy}$ ( $\times 10^6$ N/m <sup>2</sup> )	$\sigma_{yz}$ ( $\times 10^6$ N/m <sup>2</sup> )	$D_x$ ( $\times 10^{-5}$ C/m <sup>2</sup> )	$H_{zx}$ ( $\times 10^6$ N/m <sup>2</sup> )
$f=-2$	17.82169	253.15140	176.09748	84.28616	167.14326	10.62253
$f=-1$	17.47606	186.18140	129.51173	74.85472	127.66655	9.43236
$f=0$	17.04978	136.23004	94.76450	66.72413	106.49902	8.41160
$f=1$	16.54391	99.14103	68.96460	59.42338	98.78756	7.51470
$f=2$	15.96466	72.62349	50.65202	53.11115	84.35466	6.74578

are extended. More specifically, the absolute values of phason displacement increase as the gradient factor in the QCs layers increases under mechanical load. The insensitive points of phonon field stress and electric potential are observed in the QCs layer. Furthermore, the changes of the quantities along the thickness direction also are affected by the stacking sequence. When the top surface is subjected to an electric displacement, in particular, the amplitudes of physical components in a QCs-core-layer plate are smaller than those in a QCs-skin-layer plate. This is valuable for the practical design of FG PQC structures that feature heterogeneous material properties.

## References

- Alibeigloo A, 2018. Thermo elasticity solution of functionally graded, solid, circular, and annular plates integrated with piezoelectric layers using the differential quadrature method. *Mechanics of Advanced Materials and Structures*, 25(9):766-784.  
<https://doi.org/10.1080/15376494.2017.1308585>
- Altay G, Dökmeçi MC, 2012. On the fundamental equations of piezoelectricity of quasicrystal media. *International Journal of Solids and Structures*, 49(23-24):3255-3262.  
<https://doi.org/10.1016/j.ijsolstr.2012.06.016>
- Chan KC, Qu NS, Zhu D, 2002. Fabrication of graded nickel-quasicrystal composite by electrodeposition. *Transactions of the IMF*, 80(6):210-213.  
<https://doi.org/10.1080/00202967.2002.11871470>
- Chen WQ, Lee KY, 2003. Alternative state space formulations for magnetoelectric thermoelasticity with transverse isotropy and the application to bending analysis of nonhomogeneous plates. *International Journal of Solids and Structures*, 40(21):5689-5705.  
[https://doi.org/10.1016/S0020-7683\(03\)00339-1](https://doi.org/10.1016/S0020-7683(03)00339-1)
- Ding DH, Yang WG, Hu CZ, et al., 1993. Generalized elasticity theory of quasicrystals. *Physical Review B*, 48(10):7003-7010.  
<https://doi.org/10.1103/PhysRevB.48.7003>
- Dubois JM, 2005. Useful Quasicrystals. World Scientific, Singapore, Singapore, p.45-56.
- Fan TY, 2010. Mathematical Theory of Elasticity of Quasicrystals and Its Applications. Science Press, Beijing, China, p.118-120 (in Chinese).
- Fan TY, 2013. Mathematical theory and methods of mechanics of quasicrystalline materials. *Engineering*, 5(4):407-448.  
<https://doi.org/10.4236/eng.2013.54053>
- Fujiwara T, de Laissardière GT, Yamamoto S, 1994. Electronic structure and electron transport in quasicrystals. *Materials Science Forum*, 150-151:387-394.  
<https://doi.org/10.4028/www.scientific.net/msf.150-151.387>
- Gao Y, Zhao BS, 2009. General solutions of three-dimensional problems for two-dimensional quasicrystals. *Applied Mathematical Modelling*, 33(8):3382-3391.  
<https://doi.org/10.1016/j.apm.2008.11.001>
- Guo JH, Chen JY, Pan EN, 2016. Size-dependent behavior of functionally graded anisotropic composite plates. *International Journal of Engineering Science*, 106:110-124.  
<https://doi.org/10.1016/j.ijengsci.2016.05.008>
- Hu CZ, Wang RH, Ding DH, et al., 1997. Piezoelectric effects in quasicrystals. *Physical Review B*, 56(5):2463-2468.  
<https://doi.org/10.1103/PhysRevB.56.2463>
- Hu WF, Liu YH, 2015. A new state space solution for rectangular thick laminates with clamped edges. *Chinese Journal of Theoretical and Applied Mechanics*, 47(5):762-771 (in Chinese).  
<https://doi.org/10.6052/0459-1879-15-033>
- Levinson M, Cooke DW, 1983. Thick rectangular plates—I: the generalized Navier solution. *International Journal of Mechanical Sciences*, 25(3):199-205.  
[https://doi.org/10.1016/0020-7403\(83\)90093-0](https://doi.org/10.1016/0020-7403(83)90093-0)
- Li LH, Liu GT, 2012. Stroh formalism for icosahedral quasicrystal and its application. *Physics Letters A*, 376(8-9):987-990.  
<https://doi.org/10.1016/j.physleta.2012.01.027>
- Li XF, Xie LY, Fan TY, 2013. Elasticity and dislocations in quasicrystals with 18-fold symmetry. *Physics Letters A*, 377(39):2810-2814.  
<https://doi.org/10.1016/j.physleta.2013.08.033>
- Li XY, Ding HJ, Chen WQ, 2006. Pure bending of simply supported circular plate of transversely isotropic functionally graded material. *Journal of Zhejiang University SCIENCE A*, 7(8):1324-1328.  
<https://doi.org/10.1631/jzus.2006.A1324>
- Li XY, Li PD, Wu TH, et al., 2014. Three-dimensional fundamental solutions for one-dimensional hexagonal quasicrystal with piezoelectric effect. *Physics Letters A*, 378(10):826-834.  
<https://doi.org/10.1016/j.physleta.2014.01.016>
- Li Y, Yang LZ, Gao Y, 2017. An exact solution for a functionally graded multilayered one-dimensional orthorhombic quasicrystal plate. *Acta Mechanica*, in press.  
<https://doi.org/10.1007/s00707-017-2028-8>
- Louzguine-Luzgin DV, Inoue A, 2008. Formation and properties of quasicrystals. *Annual Review of Materials Research*, 38:403-423.  
<https://doi.org/10.1146/annurev.matsci.38.060407.130318>
- Mikaeeli S, Behjat B, 2016. Three-dimensional analysis of thick functionally graded piezoelectric plate using EFG method. *Composite Structures*, 154:591-599.  
<https://doi.org/10.1016/j.compstruct.2016.07.067>
- Móricz F, 1989. On  $\Lambda^2$ -strong convergence of numerical sequences and Fourier series. *Acta Mathematica Hungarica*,

- 54(3-4):319-327.  
<https://doi.org/10.1007/BF01952063>
- Pan E, Han F, 2005. Exact solution for functionally graded and layered magneto-electro-elastic plates. *International Journal of Engineering Science*, 43(3-4):321-339.  
<https://doi.org/10.1016/j.ijengsci.2004.09.006>
- Qing GH, Wang L, Zhang XH, 2017. Analytical solution of composite laminates with two opposite sides clamped and other sides free boundary. *Machinery Design & Manufacture*, (2):161-164 (in Chinese).  
<https://doi.org/10.3969/j.issn.1001-3997.2017.02.045>
- Shechtman D, Blech I, Gratias D, et al., 1984. Metallic phase with long-range orientational order and no translational symmetry. *Physical Review Letters*, 53(20):1951-1953.  
<https://doi.org/10.1103/PhysRevLett.53.1951>
- Sheng HY, Wang H, Ye JQ, 2007. State space solution for thick laminated piezoelectric plates with clamped and electric open-circuited boundary conditions. *International Journal of Mechanical Sciences*, 49(7):806-818.  
<https://doi.org/10.1016/j.ijmecsci.2006.11.012>
- Sladek J, Sladek V, Pan E, 2013. Bending analyses of 1D orthorhombic quasicrystal plates. *International Journal of Solids and Structures*, 50(24):3975-3983.  
<https://doi.org/10.1016/j.ijsolstr.2013.08.006>
- Sun TY, Guo JH, Zhang XY, 2018. Static deformation of a multilayered one-dimensional hexagonal quasicrystal plate with piezoelectric effect. *Applied Mathematics and Mechanics (English Edition)*, 39(3):335-352.  
<https://doi.org/10.1007/s10483-018-2309-9>
- Suresh S, Mortensen A, 1998. Fundamentals of Functionally Graded Materials: Processing and Thermomechanical Behavior of Graded Metals and Metal-ceramic Composites. IOM Communications, London, UK, p.156-163.
- Timoshenko SP, Goodier JN, 1970. Theory of Elasticity. McGraw-Hill, New York, USA, p.78-82.
- Wang JG, Chen LF, Fang SS, 2003. State vector approach to analysis of multilayered magneto-electro-elastic plates. *International Journal of Solids and Structures*, 40(7):1669-1680.  
[https://doi.org/10.1016/S0020-7683\(03\)00027-1](https://doi.org/10.1016/S0020-7683(03)00027-1)
- Wang X, Zhang JQ, Guo XM, 2005. Two kinds of contact problems in decagonal quasicrystalline materials of point group 10 mm. *Acta Mechanica Sinica*, 37(2):169-174 (in Chinese).  
<https://doi.org/10.3321/j.issn:0459-1879.2005.02.007>
- Xu WS, Wu D, Gao Y, 2017. Fundamental elastic field in an infinite plane of two-dimensional piezoelectric quasicrystal subjected to multi-physics loads. *Applied Mathematical Modelling*, 52:186-196.  
<https://doi.org/10.1016/j.apm.2017.07.014>
- Yang B, Ding HJ, Chen WQ, 2012. Elasticity solutions for functionally graded rectangular plates with two opposite edges simply supported. *Applied Mathematical Modelling*, 36(1):488-503.  
<https://doi.org/10.1016/j.apm.2011.07.020>
- Yang LZ, Gao Y, Pan EN, et al., 2015. An exact closed-form solution for a multilayered one-dimensional orthorhombic quasicrystal plate. *Acta Mechanica*, 226(11):3611-3621.  
<https://doi.org/10.1007/s00707-015-1395-2>
- Yaslan HÇ, 2013. Equations of anisotropic elastodynamics in 3D quasicrystals as a symmetric hyperbolic system: deriving the time-dependent fundamental solutions. *Applied Mathematical Modelling*, 37(18-19):8409-8418.  
<https://doi.org/10.1016/j.apm.2013.03.039>
- Ying J, Lü CF, Lim CW, 2009. 3D thermoelasticity solutions for functionally graded thick plates. *Journal of Zhejiang University SCIENCE A*, 10(3):327-336.  
<https://doi.org/10.1631/jzus.A0820406>
- Zhao MH, Dang HY, Fan CY, et al., 2017. Analysis of a three-dimensional arbitrarily shaped interface crack in a one-dimensional hexagonal thermo-electro-elastic quasicrystal bi-material. Part I: theoretical solution. *Engineering Fracture Mechanics*, 179:59-78.  
<https://doi.org/10.1016/j.engfracmech.2017.04.019>
- Zhao MH, Li Y, Fan CY, et al., 2018. Analysis of arbitrarily shaped planar cracks in two-dimensional hexagonal quasicrystals with thermal effects. Part I: theoretical solutions. *Applied Mathematical Modelling*, 57:583-602.  
<https://doi.org/10.1016/j.apm.2017.07.023>
- Zhou YB, Li XF, 2018. Two collinear mode-III cracks in one-dimensional hexagonal piezoelectric quasicrystal strip. *Engineering Fracture Mechanics*, 189:133-147.  
<https://doi.org/10.1016/j.engfracmech.2017.10.030>

## 中文概要

**题目:** 基于状态向量法分析功能梯度一维六方压电准晶层合板的静态响应

**目的:** 功能梯度准晶材料有助于减缓层合板界面处的应力集中现象, 提高层间粘接强度, 从而提升层合板表面的耐磨性。本文旨在建立功能梯度压电准晶层合板的力学模型, 并研究功能梯度变化和叠放顺序对层合板的影响。

**创新点:** 1. 首次将状态向量法推广到功能梯度压电准晶板的分析中; 2. 假设功能梯度函数的变化形式为幂函数和指数函数; 3. 在准晶层中观察到声子场应力和电势的不敏感点。

**方法:** 1. 通过联立三大基本方程, 推导出准晶板的状态方程, 并求解该微分方程, 得到单层准晶板的解析解; 2. 通过引入功能梯度函数, 使解析解中的描述各材料特性的值能够沿厚度方向呈现梯度

变化; 3. 采用传递矩阵法, 求出多层准晶板的解析解; 4. 通过仿真模拟, 将所得结果与已有文献进行对比, 验证所提方法的可行性和有效性。

**结论:** 1. 准晶层合板中的功能梯度效应随着梯度参数的增加而增大, 且材料参数的变化对声子场、相位子场以及电场的响应均产生影响。2. 在功能梯度

效应下, 从准晶层中观察到了声子场应力和电势的不敏感点。3. 与准晶作为中间层相比, 准晶作为表层时机械载荷引起的位移响应更小。研究结果可以为压电准晶元器件的设计提供理论参考。

**关键词:** 状态向量法; 功能梯度准晶; 压电; 板